JOURNAL OF CATALYSIS 84, 135–144 (1983)

Deactivation of Nickel Methanation Catalysts Induced by the Decomposition of Iron Carbonyl

II. Interactions between Iron and Nickel

WEI-MING SHEN[1] AND J. A. DUMESIC[2]

Department of Chemical Engineering, University of Wisconsin, Madison, Wisconsin 53706

Received February 1, 1983; revised June 22, 1983

Catalysts prepared by thermally decomposing $Fe(CO)_5$ on Al_2O_3 powder or Ni/Al_2O_3 catalysts were studied using both methanation reaction kinetics measurements and *in situ* Mössbauer spectroscopy. Iron-induced shifts in the kinetic parameters of the methanation reaction over supported nickel catalysts are the consequence of both pore-mouth blocking of the alumina micropores by iron particles and the interaction of iron with nickel particles in the macropores of the support. The presence of nickel appears to facilitate the formation of zero-valent iron during the decomposition of $Fe(CO)_5$. In addition, Auger electron spectroscopy (AES) studies of model Ni/Al_2O_3 samples composed of nickel evaporated onto thin films of alumina demonstrated that, at low partial pressures, $Fe(CO)_5$ decomposes preferentially on nickel surfaces rather than on Al_2O_3. Besides pore-mouth blocking, iron-induced deactivation of nickel methanation catalysts can also be attributed to the deposition of carbon on the catalyst.

INTRODUCTION

In a previous publication (*1*), the mechanism of iron carbonyl-induced deactivation of alumina-supported nickel methanation catalysts was investigated using both reaction kinetics measurements and *in situ* Mössbauer spectroscopy. It was concluded that the iron-induced decrease in methanation activity of Ni/Al_2O_3 catalysts was due primarily to blocking of micropores by the Fe particles formed during the diffusion-limited decomposition of iron carbonyl. In this paper, attention is focused on assessing both the contribution of iron deposits to the catalytic activity and the importance of interactions between iron and nickel in shifting the kinetic properties of these iron-deactivated nickel methanation catalysts. For these purposes, methanation kinetics measurements and *in situ* Mössbauer spectroscopy studies were carried out on samples prepared by depositing different distributions of iron on Ni/Al_2O_3 and Al_2O_3. In addition, Auger electron spectroscopy studies on low surface area, model samples were conducted to provide direct evidence for the interaction between Ni particles and Fe deposited from the decomposition of $Fe(CO)_5$.

EXPERIMENTAL

Preparation of High Surface Area Catalysts with Different Iron Distributions

In run AlFe-1, iron was deposited onto γ-Al_2O_3 powder (Davison, SMR-7, 170/200 mesh) via $Fe(CO)_5$ decomposition following the same procedure used in the previous study of iron-induced deactivation of Ni/Al_2O_3 methanation catalysts (*1*). In short, the Al_2O_3 (0.25 g) was placed in a Mössbauer spectroscopy cell, described elsewhere (*2*), which also served as a methanation reactor. The sample was then given three consecutive doses of $^{57}Fe(CO)_5$, for a total of 9.6 h, under methanation reaction conditions (using the procedure from run NiFe-3 in the previous paper (*1*): tempera-

[1] Present address: Union Carbide Corp., Parma Technical Center, P.O. Box 6116, Cleveland, Ohio 44101.

[2] Author to whom correspondence should be addressed.

0021-9517/83 $3.00

ture of 620–650 K, total pressure near 0.15 MPa, and H_2:CO = 7:1).

The catalyst preparation for run AlFe-2 was essentially the same as that for run AlFe-1, except for a 1-h *in situ* treatment in H_2O-containing gases prior to each dose of $Fe(CO)_5$. Specifically, 0.25 g of a 5.74 wt% Ni/Al_2O_3 catalyst (the preparation of which has been described in Ref. (*1*)) was placed in a "prereactor" upstream from the Mössbauer spectroscopy cell (*2*) containing the γ-Al_2O_3 powder. Both the Al_2O_3 and the Ni/Al_2O_3 catalyst were first heated in flowing H_2 to 723 K using the temperature schedule described elsewhere (*3*). Prior to each dose of $Fe(CO)_5$, synthesis gas ($H_2:CO = 7:1$ and total pressure near 0.15 MPa) was passed through the reactor network for 1 h with both the prereactor and the Mössbauer spectroscopy cell at ca. 620 K. By controlling the CO conversion in the prereactor (via adjustment of the prereactor temperature), the Al_2O_3 powder in the cell could be conditioned in a H_2O-containing atmosphere similar to that which existed in previous deactivation studies of Ni/Al_2O_3 (*1*). (The H_2O content was typically 0.90–1.25%.) The prereactor was then bypassed and the Al_2O_3 powder was dosed with $^{57}Fe(CO)_5$ for 2 h. This H_2O treatment and $Fe(CO)_5$ dosing procedure were repeated three times (for a total of 6 h $Fe(CO)_5$ treatment) before the Fe-deposited Al_2O_3 powder was characterized using Mössbauer spectroscopy.

In run NiFe-U, a uniform distribution of iron was deposited on the Ni/Al_2O_3 catalyst in the following manner. The 5.74 wt% Ni/Al_2O_3 catalyst (ca. 1 g) was loaded into a pyrex sample cell and dried under vacuum at 393 K. After cooling to room temperature under vacuum, $Fe(CO)_5$ vapor (ca. 60 μmol) with the natural abundance of ^{57}Fe (2.2%) was admitted to the sample cell. Adsorption was then allowed to proceed for several minutes. The sample cell was subsequently heated to 380 K at the same time that the cell was being evacuated with a roughing pump. This thermal decomposition of $Fe(CO)_5$ was carried out overnight. The all-glass vacuum systems used for $Fe(CO)_5$ handling and thermal decomposition have been described elsewhere (*4, 5*). The iron-containing Ni/Al_2O_3 catalyst was then treated in flowing H_2 at 650 K. This treatment ensured that the adsorbed $Fe(CO)_5$ was completely decomposed, as Brenner and Hucul (*6*) have reported the formation of subcarbonyl species for $Fe(CO)_5$ on Al_2O_3 after treatment at 390 K. Passivation of the catalyst was carried out by letting air diffuse into the He-filled sample cell at room temperature. Finally, the catalyst was reduced in the Mössbauer spectroscopy cell at 650 K before methanation kinetics measurements. However, due to the low ^{57}Fe concentration on the catalyst, it was not characterized using Mössbauer spectroscopy.

Preparation and Characterization of Low Surface Area, Model Samples

The preparation of model Ni/Al_2O_3 samples is depicted schematically in Fig. 1. A high purity aluminum foil (Alfa-Ventron 99.997%) was first chemically cleaned in successive solutions of acetone, methanol, and distilled water, respectively. The foil was then chemically polished at 350 K for 3 min in a solution consisting of 100 ml H_3PO_4, 5 ml HNO_3, and 20 ml distilled water. An aluminum oxide layer was grown by anodization of the polished aluminum foil at 22.5 V in 3 wt% ammonium tartrate solution (pH = 7, maximum current density = 1 mA/cm^2). This treatment produced a nonporous alumina layer with a thickness of about 30 nm (*7*). To convert this amorphous alumina layer to γ-alumina, the foil was further treated in oxygen at 870 K for 20 h (*7*).

Two or three segments (ca. 15 by 8 mm each) of the oxidized foil were placed in a vacuum metal evaporator. With one-half of each segment covered by a glass microscope slide, the samples were simultaneously coated with approximately 1.5 nm

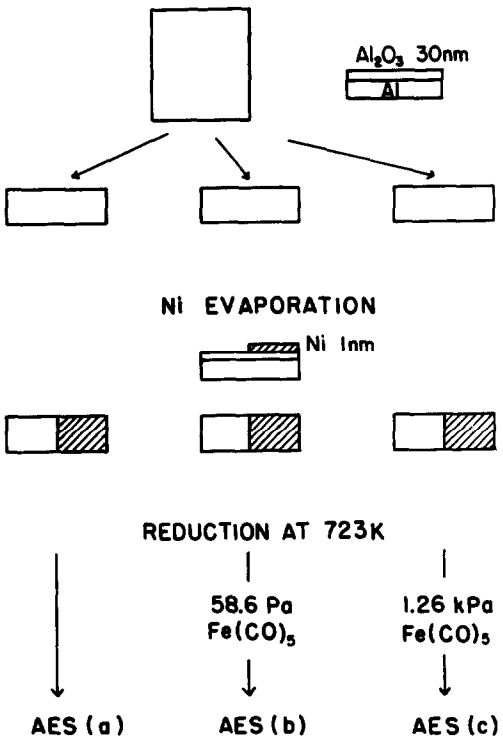

FIG. 1. Schematic preparation of model Ni/Al_2O_3 samples. The corresponding Auger electron spectra are shown in Fig. 4.

of nickel at a background pressure of ca. 5 $\times 10^{-5}$ Pa. Thus, for each segment, one-half of the sample was covered with a nickel overlayer to model a Ni/Al_2O_3 catalyst, while the other half was free of Ni and served as an Al_2O_3 control (see Fig. 1). These segments were then treated in flowing H_2 at 720 K for 2.5 h, and they were then subjected to various $Fe(CO)_5$ treatments as described for run NiFe-U (also see Fig. 1). They were subsequently passivated at room temperature, by allowing air to diffuse into the sample cell, and transferred to an Auger electron spectrometer for surface characterization.

Auger electron spectroscopy (AES) studies on the above model samples were carried out in a Physical Electronics model 548 ESCA/AES spectrometer. The electron takeoff angle (relative to sample surface) of the sample holder was 33°.

Characterization and Methanation Studies of High Surface Area Catalysts

In situ Mössbauer spectroscopy and methanation kinetics measurements were carried out as described elsewhere (*1*). All methanation activities reported in this paper are per gram of catalyst. This is done to assess the contribution of iron to the catalytic activity of the above series of related catalysts. BET surface area measurements were made using an all-glass, high-vacuum system. This was done volumetrically by dosing known amounts of N_2 into a glass cell containing the sample and simultaneously measuring the gas phase pressure, as described previously (*8*).

RESULTS

Methanation Kinetics

The methanation activity of catalyst AlFe-1 was significantly lower than that for an iron-deactivated Ni/Al_2O_3 catalyst containing about the same amount of iron. In particular, the 5.74 wt% Ni/Al_2O_3 catalyst dosed for 9.7 h with $Fe(CO)_5$ contained about 0.21 wt% Fe (run NiFe-3 in a previous publication (*1*)), and its methanation activity was about 1 μmol $CH_4/g \cdot$ sec at ca. 650 K ($H_2:CO = 7:1$, and total pressure of 0.15 MPa), while the methanation activity of catalyst AlFe-1 (Al_2O_3 powder dosed with $Fe(CO)_5$ for 9.6 h) was about 0.18 μmol $CH_4/g \cdot$ sec. The absorption peak areas in the Mössbauer spectra of catalysts AlFe-1 and NiFe-3 were about the same (as will be shown in the next section), indicating that these samples had similar iron loadings. Methanation kinetic parameters for these two iron-containing catalysts are shown in Table 1. Both AlFe-1 and NiFe-3 (with 9.7 h exposure to $Fe(CO)_5$) showed essentially the same activation energy, but the reaction rate dependencies on the H_2 and CO partial pressures were significantly different. After the completion of run AlFe-1, it was noted that the decomposition of $Fe(CO)_5$ was not uniform throughout the catalyst bed. That is, the top of the

TABLE 1

Kinetic Parameters[a] of Iron-containing Catalysts Formed by $Fe(CO)_5$ Decomposition

	E_A(kJ/mol)	X	Y
Run NiFe-3			
Fresh Ni/Al_2O_3	120	0.74	0.11
4.5 h treatment with $Fe(CO)_5$	91	0.89	0.06
7.0 h treatment with $Fe(CO)_5$	77	1.04	0.04
9.7 h treatment with $Fe(CO)_5$	70	1.03	0.10
Run NiFe-U (uniform Fe deposit on Ni/Al_2O_3)	89	0.69	0.16
Run AlFe-1 (Fe deposited on Al_2O_3)	71	1.78	−0.41

[a] $r_{CH_4} = A \exp(-E_A/RT)\, P_{H_2}{}^X P_{CO}{}^Y$.

bed (in the downflow reactor) was black due to the deposited iron, while the Al_2O_3 powder in the bottom of the catalyst bed was still white at the end of the run.

Chemical analyses (Galbraith Laboratories) indicated that the Fe/Ni ratio of the catalyst in run NiFe-U was 0.034. This value is comparable with those values (0.01–0.10) characteristic of iron-deactivated Ni/Al_2O_3 catalysts (NiFe catalysts) reported earlier (*1*). Thus, the only difference between this catalyst (NiFe-U) and other NiFe catalysts is the distribution of the Fe deposited within the Al_2O_3 support granules. With $Fe(CO)_5$ being first adsorbed and then thermally decomposed, the NiFe-U catalyst is expected to have a more uniform Fe distribution than the NiFe catalysts which were prepared by exposing Ni/Al_2O_3 catalysts to $Fe(CO)_5$ under methanation reaction conditions. The methanation activity of the NiFe-U catalyst was more than an order of magnitude higher than the activities of the latter NiFe catalysts containing comparable amounts of Fe. In fact, its activity was ca. 15–20% higher than that of a fresh, iron-free Ni/Al_2O_3 catalyst. Kinetic parameters for the methanation reaction over this NiFe-U catalyst are tabulated in Table 1. It can be seen that the methanation kinetics over this catalyst are different from those of either a fresh, iron-free nickel catalyst or an iron-deactivated Ni catalyst with a comparable amount of Fe.

Catalyst Characterization Using Mössbauer Spectroscopy

Room temperature Mössbauer spectra of AlFe catalysts quenched from methanation reaction conditions are shown in Fig. 2. Also included in this figure is the spectrum of the iron-deactivated Ni/Al_2O_3 catalyst used in run NiFe-3. As discussed elsewhere (*1*), these spectra can be characterized in terms of three Fe-containing components: iron-carbide (χ-carbide) and Fe^{2+} in the catalyst sample, and iron impurities in the Be windows of the Mössbauer spectroscopy cell. However, as can be seen in Fig. 2, there is a quantitative difference between

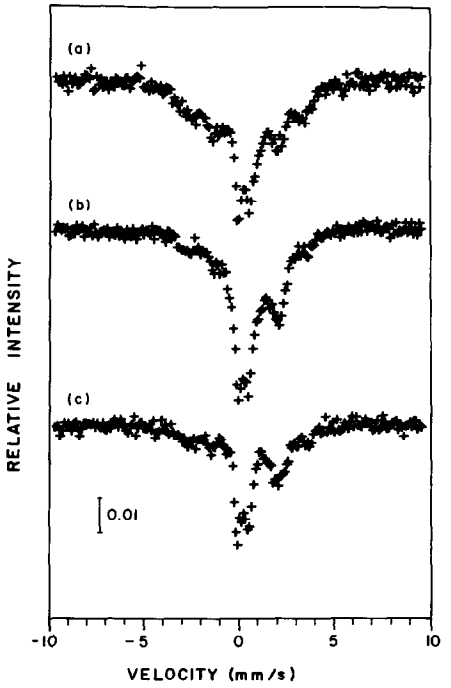

FIG. 2. Room temperature Mössbauer spectra of samples quenched from methanation reaction conditions. Isomer shifts are relative to metallic iron. (a) 5.74% Ni/Al_2O_3 catalyst after 9.7 h exposure to $^{57}Fe(CO)_5$ in three doses (run NiFe-3). (b) Al_2O_3 after 9.6 h exposure to $^{57}Fe(CO)_5$ in three doses (run AlFe-1). (c) Al_2O_3 pretreated in H_2O-containing atmosphere and exposed to $^{57}Fe(CO)_5$ for 6 h in three doses (run AlFe-2).

the spectra of the AlFe catalysts and that of catalyst NiFe-3: the absorption peak at +2.0 mm/s Doppler velocity is more prominent in the AlFe catalysts. Accordingly, the concentration of Fe^{2+} is higher in the AlFe catalysts than in the iron-deactivated Ni/Al_2O_3 catalyst.

Room temperature Mössbauer spectra of catalyst samples after H_2 treatment at reaction temperatures (ca. 650 K) are shown in Fig. 3. For comparison, the spectrum of the NiFe-3 catalyst after H_2 treatment is also included in this figure. Computer fitting of these spectra was carried out as previously described (*1*). These spectra show contributions from four iron-containing species: ferromagnetic metallic iron, Fe^{2+}, and a broad singlet due to Fe^0 in the sample, and iron impurities in the beryllium windows. The solid lines represent computer-fitted spectra, and the corresponding Mössbauer parameters of these spectra are summarized in Table 2. As in the case of the spectra reported in the previous publication (*1*), it was necessary to add the broad spectral singlet near zero Doppler velocity to obtain good computer fits of these spectra.

The above assertion that the catalysts of runs AlFe-1 and NiFe-3 (both exposed to $Fe(CO)_5$ for 9.7 h) contained similar amounts of iron is verified by their total spectral areas. As can be seen in Table 2,

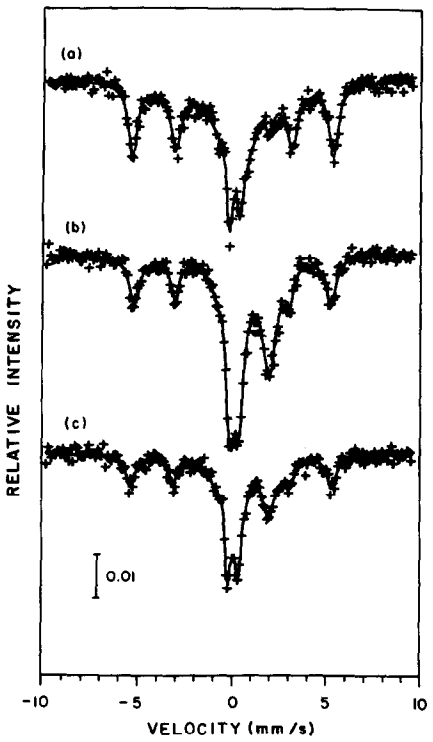

FIG. 3. Room temperature Mössbauer spectra of samples after H_2 treatment at ca. 650 K. The results of computer fitting are indicated by solid lines. Isomer shifts are relative to metallic iron. (a) 5.74% Ni/Al_2O_3 catalyst after 9.7 h exposure to $^{57}Fe(CO)_5$ in three doses (run NiFe-3). (b) Al_2O_3 after 9.6 h exposure to $^{57}Fe(CO)_5$ in three doses (run AlFe-1). (c) Al_2O_3 pretreated in H_2O-containing atmosphere and exposed to $^{57}Fe(CO)_5$ for 6 h in three doses (run AlFe-2).

TABLE 2

Mössbauer Parameters of Spectra Shown in Fig. 3

Fe-containing phases	Fe/Be[a]	Spectral area[b] (%)	Mössbauer parameters[c]
	Spectrum (a) (run NiFe-3)		
Ferromagnetic metallic iron	5.28	64.0	H = 332 kOe QS = −0.021 mm/s IS = 0.006 mm/s
Fe^{2+}	0.52	6.3	QS = 2.017 mm/s IS = 0.910 mm/s
Fe^0 (broad singlet)	2.54	29.7	IS = 0.257 mm/s
	Spectrum (b) (run AlFe-1)		
Ferromagnetic metallic iron	2.78	38.0	H = 324 kOe QS = 0.023 mm/s IS = 0.008 mm/s
Fe^{2+}	4.16	56.8	QS = 1.832 mm/s IS = 1.066 mm/s
Fe^0 (broad singlet)	0.38	5.1	IS = −0.035 mm/s
	Spectrum (c) (run AlFe-2)		
Ferromagnetic metallic iron	2.31	49.3	H = 331 kOe QS = 0.008 mm/s IS = −0.008 mm/s
Fe^{2+}	2.15	45.9	QS = 1.879 mm/s IS = 1.063 mm/s
Fe^0 (broad singlet)	0.22	4.7	IS = −0.126 mm/s

[a] The spectral area of the phase of interest normalized by the area of the iron impurities in the Be windows.

[b] Relative spectral areas calculated excluding the contributions from the iron impurities in the Be windows.

[c] H, QS, and IS are the computer-fitted magnetic hyperfine field, quadrupole splitting, and isomer shift. All isomer shifts are relative to metallic iron at room temperature.

the total Mössbauer spectral areas for iron species in these catalysts (normalized by the constant spectral area of the iron impurities in the Be windows) are 8.34 and 7.32 for runs NiFe-3 and AlFe-1, respectively. In addition, the previous statement that the AlFe catalysts contained higher concentrations of Fe^{2+} than the catalyst of run NiFe-3 is substantiated by the relative spectral areas tabulated in Table 2. Approximately 50% of the Fe deposited on Al_2O_3 was present as Fe^{2+}, while the corresponding fraction on the Ni/Al_2O_3 catalysts was only 6%. This difference cannot be attributed to the effect of surface hydroxyl groups since the treatment in H_2O-containing gases prior to each dose of $Fe(CO)_5$ (run AlFe-2) had a minor effect on the relative amount of Fe^{2+} in the catalyst (see Table 2).

In contrast to the trend for Fe^{2+}, the spectral area of the broad singlet due to Fe^0 was higher in the NiFe catalyst than in the AlFe catalysts (30 vs 5%, respectively). In addition, while this singlet had a positive isomer shift in the NiFe catalysts (0.25–0.30 mm/s (*1*)), it gave rise to a slightly negative isomer shift in AlFe catalysts (ca. −0.10 mm/s). This difference may be indicative of a difference in chemical states for the Fe^0 species present on these two series of catalysts.

AES Characterization of Model Samples

Auger electron spectra of model Ni/Al_2O_3 samples are shown in Fig. 4. The various catalyst treatments given to each sample are summarized in the figure caption. Spectra obtained from both the Ni and Al_2O_3 halves of the sample are included. The assignment of the major spectral peaks is indicated by means of the stick diagrams. As can be seen in this figure, $Fe(CO)_5$ was preferentially decomposed on the Ni surface when its partial pressure was low. However, at higher partial pressures, the decomposition of $Fe(CO)_5$ occurred equally on both halves of the sample.

The attenuation factor for the Al Auger electrons at 1396 eV due to Ni and/or Fe

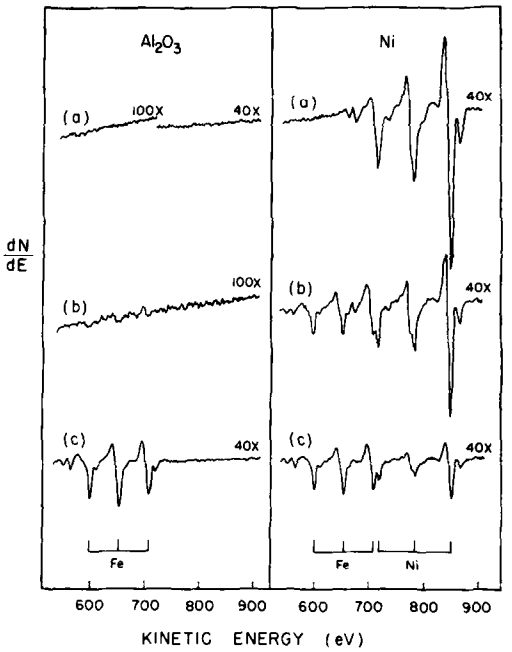

FIG. 4. Auger electron spectra of the Ni and Al_2O_3 halves of model Ni/Al_2O_3 samples. (a) Sample reduced in H_2 at 723 K. (b) Sample reduced in H_2 at 723 K and exposed to $Fe(CO)_5$ at 58.6 Pa and room temperature. Sample was then heated to 380 K, followed by treatment in flowing H_2 at 650 K. (c) Sample reduced in H_2 at 723 K and exposed to $Fe(CO)_5$ at 1.26 kPa and room temperature. Sample was then heated to 380 K, followed by treatment in flowing H_2 at 650 K.

overlayers is $\exp[-\delta/(\lambda \sin \theta)]$ (*9*), where δ is the overlayer thickness, λ is the electron mean free path for inelastic scattering, and θ is the electron takeoff angle. The Al signal measured on the Al_2O_3 half of the sample was taken as the unattenuated signal in these calculations. The thickness of the Fe deposited on the Ni overlayer was determined by the difference in estimated thickness δ before and after treatment with $Fe(CO)_5$. For λ = 2.1 nm (*10*) and θ = 33°, the thicknesses of the Ni and Fe overlayers on the sample shown in Fig. 4b were estimated to be 0.7 nm and 0.2 nm, respectively. The estimate for the Ni overlayer thickness is in approximate agreement with the calculated value of 1.4 nm based on the operating conditions for Ni evaporation, i.e., the known distance between the metal

source and the Al_2O_3 substrate, and the amount of nickel employed as a point source.

DISCUSSION

Methanation Kinetics over Fe-Deposited Al_2O_3 and Ni/Al_2O_3

The methanation activity of an Fe/Al_2O_3 catalyst prepared by $Fe(CO)_5$ decomposition on Al_2O_3 (run AlFe-1) was only 18% of that observed for an iron-deactivated Ni/Al_2O_3 catalyst (run NiFe-3). Even after corrections for the differences in the amounts of ferromagnetic metallic iron present on these catalysts (see Table 2), this percentage was still only 36%. Hence, the balance of the methanation activity of the Fe-deactivated nickel catalyst results from Ni particles, some of which may be interacting with iron. In short, it is suggested that pore-mouth blocking of the alumina micropores by iron deposits is primarily responsible for the deactivation of Ni/Al_2O_3 catalysts induced by $Fe(CO)_5$ decomposition. In addition, Ni particles in the macropores of the support may have their catalytic properties modified by iron deposited thereon. It should also be noted that Ni particles in the lower portion of the catalyst bed (in the downflow reactor) may not be affected by iron, since the thermal decomposition of $Fe(CO)_5$ takes place preferentially in the upper portion of the bed.

In run NiFe-U, the Ni catalyst with a uniform distribution of Fe showed a methanation activity 15–20% higher than that of the fresh, iron-free nickel catalysts. This high methanation activity not only indicates that the distribution of Fe within the Al_2O_3 support was indeed uniform, but it also serves as evidence confirming that pore-mouth blocking is the origin of the previously reported (*1*) order of magnitude decrease in methanation activity when comparable amounts of Fe were incorporated into Ni/Al_2O_3 catalysts under reaction conditions. The activation energy for methanation over this uniformly deposited NiFe catalyst was about 30 kJ/mol lower than that over a fresh nickel catalyst. This decrease in activation energy cannot be attributed to diffusional limitations, since the activities of both catalysts were comparable. Hence, the catalytic properties of the Ni particles are modified by the Fe deposited via the decomposition of $Fe(CO)_5$. This Fe–Ni interaction is also noted in the *in situ* Mössbauer spectroscopy studies discussed later.

Additional insight into the nature of iron-induced deactivation of Ni/Al_2O_3 catalysts is provided by the BET surface area measurements. The BET surface area of the γ-Al_2O_3 support was determined to be 225 m^2/g, while the surface area of the AlFe-1 sample was 205 m^2/g. This decrease in BET surface area for the Fe-deposited catalyst is in agreement with pore-mouth blocking by iron particles. Several reasons may be suggested to explain why this surface area reduction appears to be rather small. First, the concentration of ferromagnetic metallic iron particles on catalyst AlFe-1 was only one-half of that on the NiFe-3 catalyst. Consequently, the decrease in surface area of the Ni/Al_2O_3 methanation catalyst upon exposure to $Fe(CO)_5$ is undoubtedly more significant than that reported for the support alone. Second, certain portions of the surface area may be accessible under static conditions, e.g., BET surface area measurements, but not readily accessible to gas molecules under dynamic conditions due to diffusional limitations, e.g., during kinetics measurements.

In summary, the methanation kinetics over Fe-deactivated Ni catalysts are dominated by Fe particles formed via $Fe(CO)_5$ decomposition, Ni particles interacting with Fe in the macropores of the catalyst, and Ni particles within catalyst granules which are unaffected by the $Fe(CO)_5$ decomposition. The contribution from Ni particles within the partially blocked micropores of the catalyst appears to be small, as suggested by the following argument.

The calculated mean free path of 40 nm at the reaction conditions is much larger than

the dimension of the micropores. Hence, Knudsen diffusion would be the mode of diffusion within the porous support (*11*). In the limit of severe diffusional limitations (as could be suggested by the decreases in activation energy), the observed reaction order with respect to CO (the limiting reactant) would be shifted to $(n + 1)/2$, where n is the true order (*11*). For Fe-free Ni/Al_2O_3 catalysts, this corresponds to an increase in the rate dependence on CO partial pressure from 0–0.1 to ca. 0.5. Since this was not observed experimentally, the decreases in activation energy upon incorporation of Fe into Ni catalysts cannot be attributed to diffusion limited kinetics resulting from Ni particles within partially blocked pores.

Fe–Ni Interactions

A modification of the catalytic properties of Ni particles by Fe deposits is indicated by the methanation kinetics over the NiFe-U catalyst, as discussed earlier. Further experimental evidence in support of this Fe–Ni interaction is discussed in this section.

Since the Fe/Ni ratio in the NiFe-U catalyst was only 0.034, the presence of an Fe–Ni interaction would require that $Fe(CO)_5$ be preferentially decomposed on Ni particles, instead of decomposing indiscriminately within the support granules. Indeed, as shown by the model Ni/Al_2O_3 catalyst studies, at low $Fe(CO)_5$ partial pressures the majority of the $Fe(CO)_5$ decomposed on the Ni surface. Thus, the decomposition of $Fe(CO)_5$ took place preferentially on the Ni particles for the NiFe-U catalyst, due to the low partial pressure of $Fe(CO)_5$ used during the preparation of this sample. However, as also indicated by the model catalyst studies, at higher $Fe(CO)_5$ partial pressures, the decomposition of $Fe(CO)_5$ becomes indiscriminate. On the basis of the AES peak intensities, the amounts of Fe deposited on the Ni and Al_2O_3 sides were found to be approximately the same (Fig. 4c). In short, depending on its partial pressure, $Fe(CO)_5$ can decompose on Ni particles and/or the Al_2O_3 support. Accordingly, the distribution of Fe within a Ni/Al_2O_3 catalyst depends on two factors: the preferential decomposition of $Fe(CO)_5$ on the Ni surface at low partial pressures, and the diffusional limitations on the decomposition process discussed earlier (*1*). The interaction of iron with Ni particles in the macropores is a consequence of the first factor, while pore-mouth blocking of the micropores results from the latter factor.

The results of catalyst characterization using Mössbauer spectroscopy indicated that the concentrations of Fe^{2+} and Fe^0 (broad singlet) were different in the NiFe and AlFe catalysts. The concentration of Fe^{2+} was higher in the Ni-free catalysts (AlFe series) than in the Ni-containing catalyst (NiFe-3), while the concentration of Fe^0 (broad singlet) followed a reverse trend (see Table 2). It has been reported that supported iron catalysts, prepared by impregnation methods with metal loadings lower than ca. 1 wt%, cannot be reduced to an oxidation state lower than Fe^{2+} (*12–14*) due to interactions with the support. The presence of surface hydroxyl groups on the support has also been shown to cause the oxidation of zero-valent metals deposited via the adsorption and subsequent decomposition of metal carbonyls (*6, 15, 16*). Hence, for the overall iron concentration of 0.2–0.5 wt% employed in this study, Fe^{2+} would be expected to predominate among the Fe-containing species. For the AlFe catalysts, Fe^{2+} was in fact the major iron component (comprising about 50% of the total Mössbauer spectral area). Yet, the observation that ferromagnetic metallic iron was also a major iron species indicates that the iron was not uniformly deposited on the Al_2O_3, i.e., the decomposition reaction was diffusion limited. On the Ni-containing catalyst (NiFe-3), however, zero-valent iron appears to be stabilized by interactions with Ni. In addition, the reducibility of iron has been shown to be enhanced by alloying with Ni (*17, 18*), Co (*18, 19*), or Pt (*14*). These effects would explain the decrease in

the amount of Fe^{2+} and the increase in the spectral area of the Fe^0 (broad singlet) for run NiFe-3 compared to the AlFe samples. The different chemical nature of this Fe^0 phase relative to its counterpart in the AlFe series is also suggested by the difference in isomer shift of this broad spectral singlet as noted earlier (Table 2). This may mean that the Fe^0 (broad singlet) is due to small metallic iron particles (less than ca. 3–5 nm in size) for AlFe samples, but due at least partially to iron interacting with Ni for NiFe catalysts. The spectral area data in Table 2 suggest that as much as 25–30% of the Fe in the NiFe catalysts may be interacting with Ni.

It is interesting to comment here that the preferential decomposition of $Fe(CO)_5$ on Ni particles provides a unique method of preparing alloy catalysts. In fact, it is likely that iron alloys with a variety of other metals could be prepared in this manner.

Carbon on NiFe Catalysts

Unmuth *et al.* (*20*) have reported that nickel does not form a carbide under methanation reaction conditions, while both Fe/SiO_2 and $Fe–Ni/SiO_2$ catalysts were carburized under similar reaction conditions. Hence, the two major iron-containing phases in the iron-deactivated Ni/Al_2O_3 catalyst, i.e., Fe particles and Fe–Ni particles, may be expected to be carburized under methanation conditions. This was confirmed by a Mössbauer spectroscopy study at liquid helium temperature of catalyst NiFe-3, where the carbide phase was identified as χ-carbide (*1*).

It has been shown elsewhere (*1*) that the activity of a Ni/Al_2O_3 methanation catalyst decreases both during exposure to $Fe(CO)_5$ and after the $Fe(CO)_5$ has been removed from the gaseous feed. This latter deactivation phenomenon may be attributed to iron-induced deposition of carbon on the catalyst. In fact, it has been reported that iron and Fe–Ni alloy particles are more susceptible to carbon deposition than are nickel particles (*20*). The restoration of a significant fraction of methanation activity for Fe-deactivated Ni catalysts by hydrogen treatment at ca. 630 K also suggests enhanced carbon deposition on these catalysts, since there was only minimal activity regeneration for Fe-free Ni/Al_2O_3 catalysts during this treatment (*1*).

CONCLUSIONS

At low $Fe(CO)_5$ partial pressures, the decomposition of $Fe(CO)_5$ occurred preferentially on Ni surfaces, rather than on Al_2O_3. However, at higher $Fe(CO)_5$ partial pressures, this decomposition occurred indiscriminately, without regard to the chemical nature of the surface. In addition, the decomposition of $Fe(CO)_5$ on porous materials at methanation temperatures is diffusion limited. As a consequence of this preferential decomposition of $Fe(CO)_5$ on Ni and these diffusional limitations, the decomposition of $Fe(CO)_5$ on Ni/Al_2O_3 catalysts results in essentially two different chemical states of iron. Under the reaction conditions employed in this study, ca. 60% of the Fe deposited on the catalyst was present as metallic Fe particles and about 25–30% was interacting with Ni particles in the macropores of the support. These Fe-modified Ni particles showed a comparable (though slightly higher) methanation activity, but different reaction kinetics, than metallic nickel. The observed methanation reaction kinetics over Fe-deactivated Ni catalysts reflect contributions from Fe particles, Ni particles, and Ni particles interacting with Fe.

The Fe particles formed during the diffusion-limited decomposition of $Fe(CO)_5$ were responsible for catalyst deactivation by means of pore-mouth blocking. Further catalyst deactivation of Fe-containing Ni/Al_2O_3 catalysts may be caused by iron-induced deposition of carbon.

ACKNOWLEDGMENTS

Financial support from Department of Energy (ET-78-G-01-3380) is gratefully acknowledged. We also thank Mr. T. F. Hayden for carrying out the Auger

electron spectroscopy studies, and Ms. S. M. Peters for measuring BET surface areas. In addition, valuable discussions with Professor C. G. Hill are gratefully acknowledged.

REFERENCES

1. Shen, W. M., Dumesic, J. A., and Hill, C. G., Jr., *J. Catal.* **84,** 119 (1983).
2. Shen, W. M., Dumesic, J. A., and Hill, C. G., Jr., *Rev. Sci. Instrum.* **52,** 858 (1981).
3. Shen, W. M., Dumesic, J. A., and Hill, C. G., Jr., *J. Catal.* **68,** 152 (1981).
4. Phillips, J., Clausen, B., and Dumesic, J. A., *J. Phys. Chem.* **84,** 1814 (1980).
5. Phillips, J., and Dumesic, J. A., *Appl. Surf. Sci.* **7,** 215 (1981).
6. Brenner, A., and Hucul, D. A., *Inorg. Chem.* **18,** 2836 (1979).
7. Ruckenstein, E., and Malhotra, M. L., *J. Catal.* **41,** 303 (1976).
8. Lund, C. R. F., Schorfheide, J. J., and Dumesic, J. A., *J. Catal.* **57,** 105 (1979).
9. Delgass, W. N., Haller, G. L., Kellerman, R., and Lunsford, J. H., "Spectroscopy in Heterogeneous Catalysis," p. 292, Academic Press, New York, 1979.
10. Wagner, C. D., Riggs, W. M., Davis, L. E., Moulder, J. F., and Mullenburg, G. E., "Handbook of X-ray Photoelectron Spectroscopy," Perkin–Elmer, Eden Prairie, Minn., 1979.
11. Hill, C. G., Jr., "An Introduction to Chemical Engineering Kinetics and Reactor Design," Wiley, New York, 1977.
12. Dumesic, J. A., and Topsøe, H., "Advances in Catalysis," Vol. 26, p. 121, Academic Press, New York, 1977.
13. Topsøe, H., Dumesic, J. A., and Mørup, S., *in* "Application of Mössbauer Spectroscopy" (R. L. Cohen, Ed.), Vol. 2, p. 55, Academic Press, New York, 1980.
14. Garten, R. L., *in* "Mössbauer Effect Methodology" (I. J. Gruverman and C. W. Seidel, Eds.), Vol. 10, Plenum, New York, 1976.
15. Hugues, F., Bussiere, P., Bassett, J. M., Commereuc, D., Chauvin, Y., Bonneviot, L., and Olivier, D., "Proceedings, 7th International Congress on Catalysis, Tokyo, Japan, 1980," p. 418.
16. Bowman, R. G., and Burwell, R. L., Jr., *J. Catal.* **63,** 463 (1980).
17. Unmuth, E. E., Schwartz, L. H., and Butt, J. B., *J. Catal.* **61,** 242 (1980).
18. Brown, R., Cooper, M. E., and Whan, D. A., *Appl. Catal.* **3,** 177 (1982).
19. Stanfield, R. M., and Delgass, W. N., *J. Catal.* **72,** 37 (1981).
20. Unmuth, E. E., Schwartz, L. H., and Butt, J. B., *J. Catal.* **63,** 404 (1980).